

PAPER • OPEN ACCESS

Experiment and simulation of fatigue crack growth of SLM nickel base superalloy with different stress ratios and building directions

To cite this article: Zhi Yuan Xue 2019 *IOP Conf. Ser.: Mater. Sci. Eng.* **490** 032036

View the [article online](#) for updates and enhancements.

Experiment and simulation of fatigue crack growth of SLM nickel base superalloy with different stress ratios and building directions

ZhiYuan Xue^{1,2,*}

¹Engineering, Nanchang Hangkong University, Nanchang 330063, China

²Jiangxi Key Laboratory of Micro Aeroengine Technology, NanChang, 330063, China

*Corresponding author e-mail:1870259117@163.com

Abstract. Building orientation and stress ratio have much affection on long fatigue crack growth for Selective Laser Melting (SLM) Inconel 625. Compact-tension (CT) specimens in different orientations were tested with stress ratios (R) of 0.1. The Fatigue Crack Growth Rate (FCGR) in Paris was influenced by the loading factor and the difference of microstructure. With the help of finite element software (Abaqus/Franc3D), the FCGR data were calculated excitedly for different directional specimens under R of 0.5. Scanning Electron Microscopy (SEM) method was also introduced to observe the fracture mechanism of FCG in Paris region.

1. Introduction

Laser-selective melting additive manufacturing technology (SLM) is one of additive manufacturing techniques. The characteristics of SLM technology include large laser energy input, the forming process is not limited by the complexity of parts, the production cycle is short, and the development cost is low[1, 2]. At present, the technology has been widely used in aerospace, biomedical and other fields[1]. Among these fields, nickel-based superalloys have received extensive attention. Taking Inconel 625 nickel-based superalloys, it is a solid solution strengthened superalloy with Ni and Cr as the matrix and Nb and Mo as the main strengthening elements.[3, 4].

However, due to some shortcomings of AM process performance, such as pores [5], unfused [6], residual stress[7], etc., it will lead to the weakening of SLM Inconel 625 in fatigue crack resistance[8]. S. Leuders et al.[5, 9] believe that the residual stress is mainly due to the steep temperature gradient and the faster cooling rate in the SLM process, while the pores and unfused are mainly due to insufficient SLM laser power[5].



In this paper, the effects of average stress and printing direction on the SLM Inconel 625 FCG rate were analyzed by experiments and finite element simulation. The experiment mainly carried out experiments and simulations on the stable crack growth stage (ie, the Paris region). Firstly, the FCG test was performed on CT samples in different directions with the stress ratio R of 0.1. Secondly, the fatigue fracture was analyzed by SEM method. Again, the ABAQUS/Franc3D was used to simulate the FCG rate of the standard CT samples in different directions under the same stress ratio (R is 0.1). The experimental and numerical analysis results were compared to confirm the degree of data matching. Finally, the numerical simulation method was used to predict the FCG stress intensity factor of SLM Inconel 625 CT specimens in different directions with other stress ratios (ie 0.5).

2. Experimental procedure

2.1 Material and specimen preparation

The process used is SLM gas atomized spherical powder technology. The morphology of the initial powder particles using SEM method is shown in Fig.1.

The elements of Inconel 625 powder were analyzed by SEM/EDS. The results show that the mass fractions (Wt %) of the main elements Cr, Mo and Ni are: 20.68 %, 8.34 % and 3.96 %, respectively. As shown in Table 1. The preparation process was carried out on a BLT-S300 machine with a vacuum chamber filled with high purity argon after evacuation in a low pressure atmosphere. In order to minimize porosity and residual stress and improve the mechanical properties of the material, an optimized SLM process is used: The laser power is 1000 W. The beam spot size was 0.1 mm. The layer thickness was about 0.04 mm.

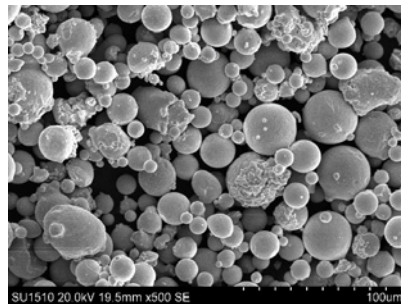


Figure 1. Powder of Inconel 625.

Table 1. Chemical compositions of Inconel 625 powder

Element	Al	C	Cr	Ti	Mo	Mn	Si
Wt%	0.37	0.014	20.68	0.2	8.34	0.04	0.14
Element	Nb	Fe	Cu	Co	Mg	S	P
Wt%	3.96	0.9	<0.01	0.17	<0.002	0.001	0.002

The size of as-received rectangular plate is 45*50*36 mm, and the microstructure of each face is shown in Fig. 2. The deposition direction of the material is in the Z-axis direction. As shown in Fig. 2b-d, the as received SLM Inconel 625 material exhibits anisotropy in microstructure and a significant austenitic character. The Z-X plane shown in Fig. 2b and the Z-Y plane shown in Fig. 2c are mainly columnar crystals. Fig. 2d is the X-Y plane, which is perpendicular to the printing direction and consists mainly of cell crystals and equiaxed crystals.

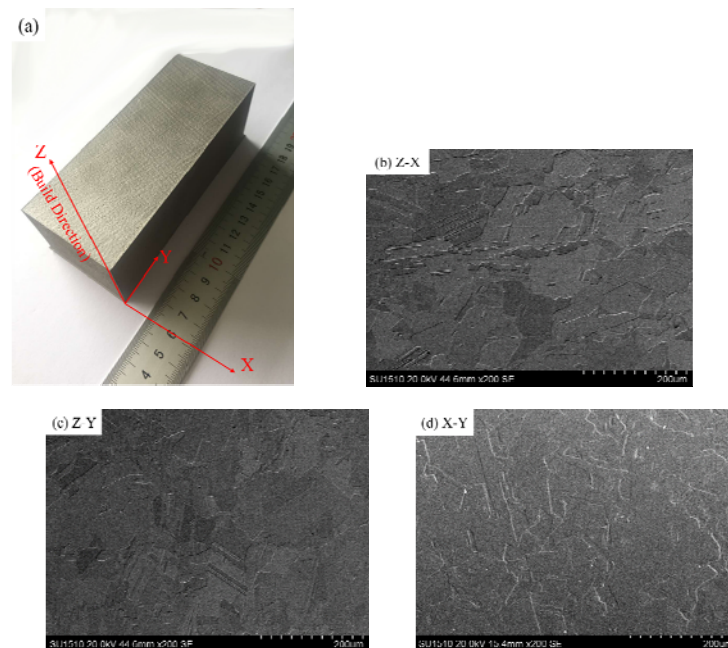
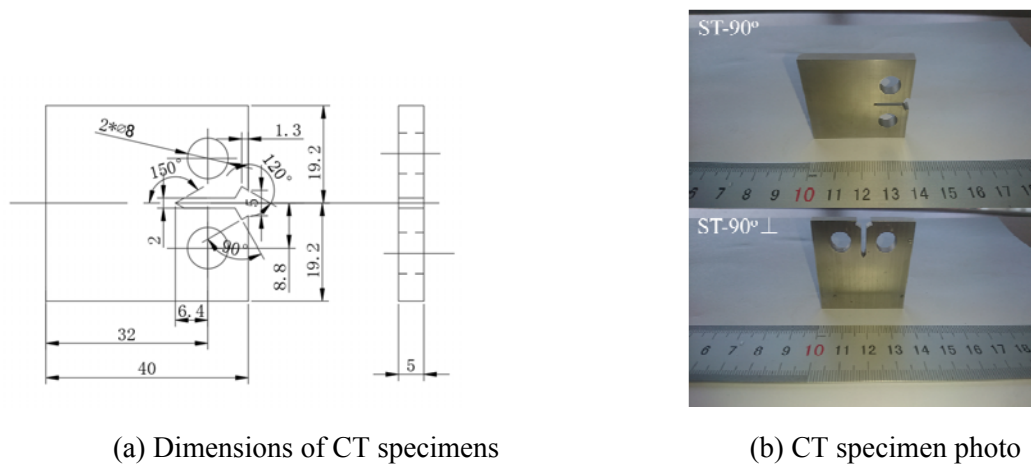


Figure 2. (a) As-received plate, (b), (c) and (d) are microstructure of each surface in as-received plate.

The geometry of the CT specimens designed in accordance with ASTM E 647 is shown in Fig. 3a. CT sample width was 40 mm, thickness was 5 mm. Two-direction CT specimens were cut from the SLM Inconel 625 plate using wire cutting machine, as shown in Fig. 3b. The crack propagation directions of the samples were perpendicular or parallel to the deposition direction (Z-axis), named ST 90° and ST $90^\circ \perp$.



(a) Dimensions of CT specimens

(b) CT specimen photo

Figure 3. Geometry of the CT specimen

2.2 Experimental procedure

K-controlled fatigue crack propagation testing with R of 0.1, 0.5 for ST- 90° specimens and ST- $90^\circ \perp$ specimens were conducted by a 5 kN Instron 8872 servo hydraulic fatigue machine. The specimen, grips and compliance gauge installation arrangement are shown in Fig. 4. The crack length was monitored as a function of cycles using the crack opening displacement (COD) compliance. The initial crack length was 9 mm.



Figure. 4. Testing system setup for FCG

The crack length measured by COD is calculated according to the following formula

$$\Delta K = \frac{\Delta P}{B\sqrt{W}} \times \frac{2+\alpha}{(1-\alpha)^{3/2}} (0.886 + 4.64\alpha - 13.32\alpha^2 + 14.72\alpha^3 - 5.6\alpha^4) \quad (1)$$

Where $\alpha = a/W$, a is the crack length and ΔP is the range of applied load amplitudes. The load waveform is the sine and the frequency is 20 Hz

3. Finite element analysis

3D FE models were developed for the same geometries of the CT specimens used in the FCG experiment, as described in section 2. The software used for the analysis is the commercial finite element code ABAQUS/Franc3D. The crack tip mesh type is shown in Fig. 5a. The model outside the sub-model is meshed by 8-noded brick element C3D8 as shown in Fig. 5a. The software automatically calculates the stress intensity factors of the crack leading edge node by M integral method. When performing crack propagation analysis, the software automatically updates the crack leading edge position and automatically re-mesh.

The simulation results of crack growth are shown in Fig. 5b ($a=14.6$ mm, $a=20.9$ mm and $a=24.23$ mm).

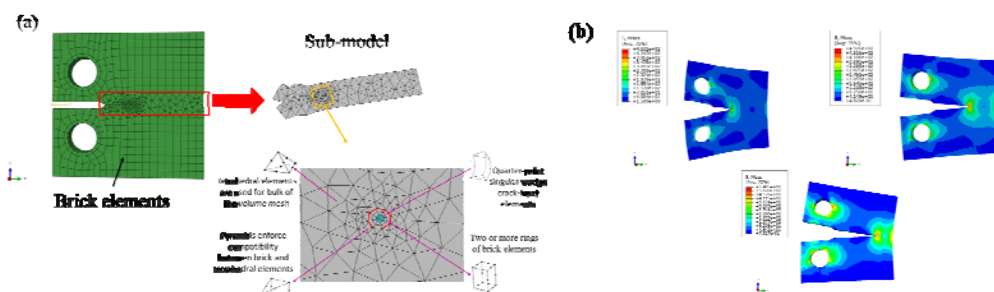


Figure. 5. Element types and simulation contours of FCG

4. Results

4.1 Fatigue crack growth data

The FCG data is summarized in a double logarithmic coordinate system, as shown in Fig. 6. From Fig. 6, the crack growth rate of ST $90^\circ \perp$ specimen is faster than that of ST 90° . In the case of $R=0.1$, the da/dN - ΔK data points of the CT samples in both directions are also obtained by ABAQUS/Franc3D, which are plotted in Fig.6. It can be seen that the experimental data and the numerical analysis data agree with each other.

Furthermore, this study predicts the FCG rate of the Paris region with stress ratios of 0.5 in both directions. The da/dN - ΔK curve is also shown in Fig. 6. It can be seen from Fig. 6 that as the stress ratio increases, the FCG rates also accelerate. Under the same R , the ST 90° direction crack growth rate is higher than the ST $90^\circ \perp$ direction, which means that the crack propagation resistance in the ST 90° direction is higher.

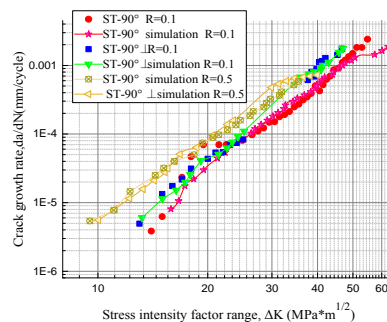


Figure. 6. FCG rate data by test and simulation at different ratio (0.1,0.5) and different orientation

4.2 Fractography

The fracture morphology of the Paris region of the fatigue crack when the stress ratio is 0.1, as shown in Fig. 7. There are fatigue steps and some secondary cracks on the fracture surface, and the number of the secondary crack in ST 90° sample fracture is slightly more than the ST $90^\circ \perp$ sample. The secondary crack consumes more crack tip strain energy and plays a certain retarding effect on crack propagation. In addition, it can be seen from Fig. 7 that a fatigue strip perpendicular to the propagate direction of the prime crack is distributed on the fracture, accompanied by intergranular tearing ribs, thereby indicating that the crack propagation mechanism is transgranular. Considering Fig. 7b and d, the fatigue strip space ($0.625\mu\text{m}$) of the ST $90^\circ \perp$ CT sample is slightly larger than the fatigue fracture fringe spacing ($0.54\mu\text{m}$) of the ST 90° CT sample. This further confirms the faster fatigue crack growth rate for the ST $90^\circ \perp$ CT sample.

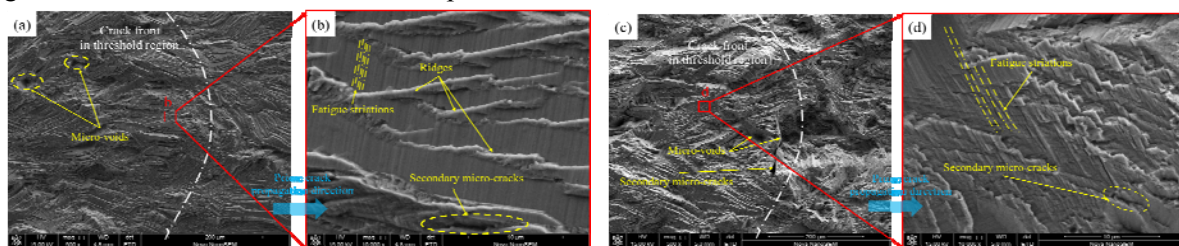


Figure. 7. SEM images of fracture morphology in the Paris region under $R = 0.1$: (a) and (b) are ST- 90° specimen. (c) and (d) are ST- $90^\circ \perp$ specimen.

5. Conclusion

The effect of building orientation and stress ratio in Paris region crack growth of Inconel 625 produced by Selective Laser Melting (SLM) method was investigated. CT specimens in two orientations (ST 90°/ST 90° ⊥) were performed under R of 0.1 to obtain the FCGR data. At the same time, the finite element CT mesh model for two directions was established by ABAQUS/Franc3D software. Some of the important conclusions can be summarized as following.

(1) Orientation dependent FCGR is observed in the Paris region. The microstructure anisotropy resulted from building process and external load have affections in Paris region. (2) The stress ratio has a strong effect on the FCG Paris region. With R increasing, the FCGR increases. At the same stress ratio, the FCGR of the ST 90° ⊥ sample is faster. (3) With the help of ABAQUS/Franc3D, it is possible to accurately simulate the effects of different stress ratios and different material directions on FCG rate.

Acknowledgments

This research was supported by The National Basic Research Program of China (No. 2015CB057400)

References

- [1] R. Konečná, L. Kunz, G. Nicoletto, A. Bača, Long fatigue crack growth in Inconel 718 produced by selective laser melting, *International Journal of Fatigue*, 92 (2016) 499-506.
- [2] J.P. Kruth, G. Levy, F. Klocke, T.H.C. Childs, Consolidation phenomena in laser and powder-bed based layered manufacturing, *CIRP Annals - Manufacturing Technology*, 56 (2007) 730-759.
- [3] G.P. Dinda, A.K. Dasgupta, J. Mazumder, Laser aided direct metal deposition of Inconel 625 superalloy: Microstructural evolution and thermal stability, *Materials Science & Engineering A*, 509 (2009) 98-104.
- [4] V. Shankar, K.B.S. Rao, S.L. Mannan, Microstructure and mechanical properties of Inconel 625 superalloy, *Journal of Nuclear Materials*, 288 (2001) 222-232.
- [5] S. Leuders, M. Thöne, A. Riemer, T. Niendorf, T. Tröster, H.A. Richard, H.J. Maier, On the mechanical behaviour of titanium alloy TiAl6V4 manufactured by selective laser melting: Fatigue resistance and crack growth performance, *International Journal of Fatigue*, 48 (2013) 300-307.
- [6] J. Günther, D. Krewerth, T. Lippmann, S. Leuders, T. Tröster, A. Weidner, H. Biermann, T. Niendorf, Fatigue life of additively manufactured Ti-6Al-4V in the very high cycle fatigue regime, *International Journal of Fatigue*, 94 (2017) 236-245.
- [7] E. Santos, Fabrication of titanium dental implants by selective laser melting, *Proceedings of SPIE - The International Society for Optical Engineering*, 5662 (2004).
- [8] A. Yadollahi, M.J. Mahtabi, A. Khalili, H.R. Doude, J.C. Newman, Fatigue life prediction of additively manufactured material: Effects of surface roughness, defect size, and shape, *Fatigue & Fracture of Engineering Materials & Structures*, (2018).
- [9] M. Shiomi, K. Osakada, K. Nakamura, T. Yamashita, F. Abe, Residual Stress within Metallic Model Made by Selective Laser Melting Process, *CIRP Annals - Manufacturing Technology*, 53 (2004) 195-198.